LETTER TO THE EDITOR

The GAPS Programme with HARPS-N@TNG

IX. The multi-planet system KELT-6: Detection of the planet KELT-6 c and measurement of the Rossiter-McLaughlin effect for KELT-6 b [★]

M. Damasso[1], M. Esposito[2,3], V. Nascimbeni[4,5], S. Desidera[4], A.S. Bonomo[1], A. Bieryla[6], L. Malavolta[4,5], K. Biazzo[7], A. Sozzetti[1], E. Covino[8], D. W. Latham[6], D. Gandolfi[9,10] M. Rainer[11], C. Petrovich[12], K. A. Collins[13,14], C. Boccato[4], R.U. Claudi[4], R. Cosentino[7,15], R. Gratton[4], A.F. Lanza[7], A. Maggio[16], G. Micela[16], E. Molinari[15,17], I. Pagano[7], G. Piotto[4,5], E. Poretti[11], R. Smareglia[18], L. Di Fabrizio[15], P. Giacobbe[1], M. Gomez-Jimenez[2,3], S. Murabito[2,3], M. Molinaro[18], L. Affer[16], M. Barbieri[19], L. R. Bedin[4], S. Benatti[4], F. Borsa[9], J. Maldonado[16], L. Mancini[20,1], G. Scandariato[7], J. Southworth[21], R. Zanmar Sanchez[7]

(Affiliations can be found after the references)

ABSTRACT

Aims. For more than 1.5 years we spectroscopically monitored the star KELT-6 (BD+31 2447), which is known to host the transiting hot-Saturn KELT-6 b, because a previously observed long-term trend in radial velocity time series suggested that there is an outer companion.
Methods. We collected a total of 93 new spectra with the HARPS-N and TRES spectrographs. A spectroscopic transit of KELT-6 b was observed with HARPS-N, and simultaneous photometry was obtained with the IAC-80 telescope.
Results. We proved the existence of an outer planet with a mininum mass $M_p \sin i = 3.71 \pm 0.21$ M_{Jup} and a moderately eccentric orbit ($e = 0.21^{+0.039}_{-0.036}$) of period P~3.5 years. We improved the orbital solution of KELT-6 b and obtained the first measurement of the Rossiter-McLaughlin effect, showing that the planet has a likely circular, prograde, and slightly misaligned orbit with a projected spin-orbit angle of $\lambda = -36 \pm 11$ degrees. We improved the KELT-6 b transit ephemeris from photometry and provide new measurements of the stellar parameters. KELT-6 appears as an interesting case for studying the formation and evolution of multi-planet systems.

Key words. (Stars:) individual: KELT-6 — Stars: planetary systems — techniques: radial velocities, photometric

1. Introduction

Analysing stellar radial velocity (RV) time series is an effective method of detecting and characterizing distant planets with orbital periods of a few years, despite the large observing time span required. To look for such companions, particularly interesting targets are stars with transiting planets, because they are an ideal laboratory for studying the architecture of multi-planet systems. In fact, the orbital geometry of the transiting planet can be described through the Rossiter-McLaughlin (RM) effect (e.g. Ohta et al. 2005) by measuring the projected spin-orbit angle and spotting the direction of the motion with respect to that of the stellar rotation. Up to now, long-term trends have been observed in the RVs of a large sample of stars with and without evidence of turnover (e.g. Knutson et al. 2014). Among them is KELT-6, a late F-type, metal-poor star (V=10.3 mag) hosting the transiting Saturn-mass planet KELT-6 b discovered by the KELT-

North survey (Collins et al. 2014, hereafter Co14). Co14 were also able to observe an unexplained residual trend in the RVs over a limited time span of 475 days. To understand the cause of this acceleration, a spectroscopic follow-up was carried out in the framework of the Global Architectures of Planetary Systems (GAPS) project[1], using the HARPS-N spectrograph (resolving power $R = 115\,000$; Cosentino et al. 2012). We also collected new RV data with the Tillinghast Reflector Echelle Spectrograph (TRES) spectrograph ($R = 44\,000$; Fűresz 2008), extending the total observing time span to 1178 days.

Together with new photometric measurements, we present results that noticeably extend knowledge about the KELT-6 system.

2. Observations and data reduction methods

We collected 71 HARPS-N spectra (exposure 900 s, typical signal-to-noise per pixel S/N~60 at 5500 Å) between 2014 February 9 and 2015 July 3, 31 of which were obtained on 2015 April 11 during a transit of KELT-6 b and used to study the RM effect. The Th-Ar simultaneous calibration was not used to avoid contamination by the lamp lines. The spectra and the RV measurements were reduced using the latest version (Nov. 2013) of the HARPS-N instrument Data Reduction Software

---

[1] http://www.oact.inaf.it/exoit/EXO-IT/Projects/Entries/2011/12/27_GAPS.html

arXiv:1508.06520v2 [astro-ph.EP] 1 Sep 2015

pipeline and applying a G2 mask. The measurement of the RVs is based on the weighted cross-correlation function (CCF) method (Baranne et al. 1996; Pepe et al. 2002).

With TRES we collected 22 spectra between 2013 December 13 and 2015 May 27. They were extracted following the procedures described by Buchhave et al. (2010). The relative RVs were derived by cross-correlating the spectra against the highest S/R spectrum in the wavelength range 4050– 5650 Å.

Simultaneously with the RM effect measurements gathered with HARPS-N, we collected the transit light curve with the IAC-80 0.82-m telescope. Data were taken from 21:18 UT to 5:32 UT, using the CAMELOT camera (E2V 2k×2k CCD; pixel scale 0.304″; field of view 10.4′ × 10.4′) and through a standard Bessell R filter. The point spread function (PSF) was intentionally defocused to a radius of ∼ 20 physical pixels to minimize flat-field residual errors and avoid detector saturation. The exposure time was set to 90 s, resulting in a net cadence of ~115 s when considering the overheads. Science frames were bias- and flat-field-corrected by standard procedures. Photometric measurements were made with the STAR-*SKY* pipeline (Nascimbeni et al. 2011, 2013). STAR*SKY* delivered the best differential light curve of KELT-6 (i.e. the one with the least scatter) using a set of four stable comparison stars (UCAC4 604-049448, UCAC4 604-049449, UCAC4 604-049450, and UCAC4 604-049454). Unfortunately, our observations were plagued by technical problems that delayed the start time of the observations, and the telescope pointing was re-adjusted, causing an offset between the first and the second halves of the light curve, which was included as a parameter in the transit model.

3. Stellar parameters

The photospheric parameters were derived with different methods from the co-added HARPS-N spectrum obtained from the out-of-transit observations (S/R∼380 per pixel at 5500 Å). We used the LTE code MOOG (Sneden 1973), along with atmospheric models (Kurucz 1992; Castelli & Kurucz 2004) and iron equivalent widths (EW). Two analyses were independently performed with the main differences being the list of iron lines and the technique used to measure EWs. In one case we used ARESv2 (Sousa et al. 2015) with the automatic continuum placement set-up and the line list from Sousa et al. (2011), adapted to the 2014 version of MOOG (Dumusque et al. 2014). In the other case, the EWs of the line list from Biazzo et al. (2012) were measured by hand using the IRAF task SPLOT, and the iron abundance was determined using the 2013 version of MOOG (see Damasso et al. 2015). In both cases, the analysis was performed differentially with respect to the Sun spectrum. We also did a third independent analysis based on the method described in Gandolfi et al. (2015). We fitted the HARPS-N spectrum to a grid of theoretical models from Castelli & Kurucz (2004), using spectral features that are sensitive to different photospheric parameters.

All the analyses gave consistent results, so we calculated their weighted averages and adopted the average of the individual uncertainties as errors. Table 1 summarizes our results. We notice that our best-fit value for T_{eff} is 170 K higher than value adopted by Co14, which was obtained from spectral synthesis modelling with Spectroscopy Made Easy (SME; Valenti & Piskunov 1996) using HIRES spectra. This difference could arise from the different analysis techniques rather than from the properties of the spectra, by noting that a well known

Table 1. Stellar parameters for the star KELT-6 derived from the analysis of the HARPS-N spectra and from stellar evolutionary tracks. Estimates from the KELT-6 b discovery paper are also listed.

Parameter	This work	Co14	Note
T_{eff} [K]	6272±61	6102±43	
$\log g$ [cgs]	4.12±0.07	$4.074^{+0.045}_{-0.070}$	
[Fe/H] [dex]	-0.27±0.06	$-0.281^{+0.039}_{-0.038}$	
Microturb. ξ [km s^{-1}]	1.49±0.1	0.85 (fixed)	
$V\sin I_\star$ [km s^{-1}]	4.53±0.26	5.0±0.5	(1)
μ linear law limb-darkening coeff.	0.48±0.14		(1)
Mass [M$_\odot$]	1.126±0.058	$1.085^{+0.043}_{-0.040}$	(2)
Radius [R$_\odot$]	$1.529^{+0.143}_{-0.137}$	$1.580^{+0.160}_{-0.094}$	(2)
Age [Gyr]	$4.90^{+0.66}_{-0.46}$	6.1±0.2	(2)
Luminosity [L$_\odot$]	3.24±0.62	$3.11^{+0.68}_{-0.39}$	(2)
Density [g cm^{-3}]	$0.44^{+0.15}_{-0.10}$	$0.387^{+0.068}_{-0.088}$	

Notes. (1) Derived from HARPS-N spectra (RM effect). (2) Matching T_{eff}, [Fe/H], and $\log g$ to the Yonsei-Yale evolutionary tracks.

bias exists in some versions of SME (Torres et al. 2012), which was removed in more recent versions (Brewer et al. 2015).

The stellar mass, radius, and age were determined by comparing our measured T_{eff}, $\log g$, and [Fe/H] with the Yonsei-Yale evolutionary tracks (Demarque et al. 2004) through the χ^2 statistics (Santerne et al. 2011). Results are listed in Table 1. The adopted errors include an extra 5% in mass and 3% in radius added in quadrature to the formal errors to take systematic uncertainties into account in the stellar models (Southworth 2011). We also employed the stellar density $\rho_\star$ derived by Co14 as a proxy of the stellar luminosity instead of $\log g$ (e.g. Sozzetti et al. 2007). The results are fully consistent with the previous findings and not more precise. We thus adopted the parameters obtained using $\log g$, finding that KELT-6 appears to be slightly less evolved than stated by Co14.

4. Improved transit ephemeris for KELT-6b

The light curve observed with the IAC-80 telescope is shown in the upper panel of Fig. 1. It has an average photometric scatter of 0.9 mmag on a 115 s timescale.

Since we could not measure the out-of-transit flux of KELT-6 to properly normalize the off-transit level of our light curve, a full, detailed modelling to extract all the orbital parameters[2] of KELT-6 b was hampered by the unsolvable degeneracy between the normalization level and the other transit parameters. Therefore we chose to fix $R_\star/a$, R_{p}/a, and i to the best-fit values published by Co14, limiting the number of free parameters to four[3]. The fit was performed with the code JKTEBOP v34 (Southworth 2008), and the associated errors were derived through 10 000 classical Monte Carlo iterations.

From the fit we could only determine the time of central transit T_{c} of KELT-6 b. We then derived an improved ephemeris (T_{c} and orbital period P) from the observed-minus-calculated diagram (lower panel of Fig. 1), by fitting both our measurement of T_{c} and the high-quality ("primary") points from Co14 through a weighted least-squares procedure, as well as an additional ephemeris obtained by the KELT team from an unpub-

[2] The fractional radii $R_\star/a$ and R_{p}/a, with $R_\star$ being the star radius, R_{p} the planet radius, and a the planet semi-major axis; the orbital inclination i; the orbital period P; the time of central transit T_0.

[3] i.e. T_0; the linear term u_1 of a quadratic limb darkening law, with the quadratic term interpolated from the Claret & Bloemen (2011) tables; the off-transit normalization level; an existing zero-point offset between the first and the second halves of the light curve.
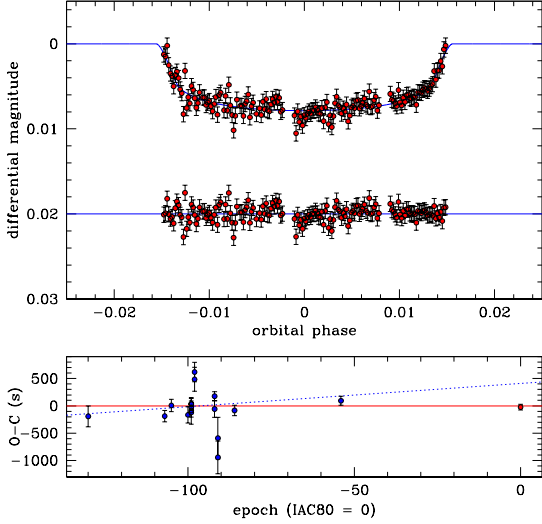
Fig. 1. *Upper panel:* KELT-6 b transit light curve (2014 Apr 11, IAC-80 telescope), and residuals from the best fit model (which is plotted with a solid blue line). The root mean square of the residuals is 0.9 mmag. *Lower panel:* $O - C$ diagram including the highest-quality measurements from C014 plus one unpublished measurement from the KELT team (blue points on the left side) and from our IAC-80 observation (red point). The $O - C$ diagram is folded on our newly determined ephemeris (solid red line), while the Co14 ephemeris is plotted with a dotted blue line.

lished transit that occurred on 2014 February 12. The results are shown in Table 4, with the reference epoch set on the most recent transit.

5. Analysis of the radial velocities

5.1. KELT-6 c comes out

The HARPS-N and TRES RVs collected for this work are listed in Tables 2 and 3, respectively. In our sample, we also included the RVs used in Co14 and collected by TRES and the High Resolution Echelle Spectrometer (HIRES) at the Keck telescope, while we excluded the first 26 HARPS-N measurements taken during the night of the KELT-6 b transit. The RV time series shows a long-term modulation with a clear turnover and a semi-amplitude higher than that of the short-period signal due to KELT-6 b (Fig. 2). KELT-6 appears to be a quiet star ($<$log(R$'_{HK}$)$>$=-4.992, $\sigma_{log(R'_{HK})}$=0.021), without evidence in the log(R$'_{HK}$) data for a modulation ascribable to an activity cycle (Fig. 3, upper plot). Besides the log(R$'_{HK}$) index, we calculated the CCF bisector span (BIS) from the HARPS-N spectra, and we found that no significant correlations exist over the timespan of the HARPS-N measurements between these datasets and the RVs with the orbital solution of KELT-6 b removed (Fig. 3, middle and lower plots). This evidence supports the hypothesis that the observed RV long-term variations are not due to the stellar activity but to an outer companion, which we name KELT-6 c and for which the data cover almost one complete orbit. This scenario is further strengthened by looking, for example, at the empirical calibrations of Santos et al. (2000) (see Eq. 2 and Fig. 6 therein) that, for a star like KELT-6, predict a RV dispersion due to activity-related phenomena at the level of $\sim$10 m s^{-1}, while our measured semi-amplitude is $\sim$3-5 times higher ($K \sim$66 m s^{-1}) once the orbital solution of KELT-6 b is removed.

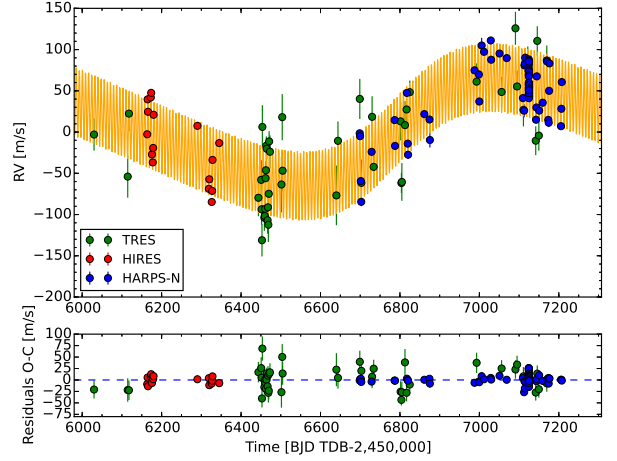**Fig. 2.** *Upper panel:* Radial velocity time series of KELT-6. The 1-σ errorbars are over-plotted to each data point. When they are not visible, this means they are smaller than the symbol size. Over-plotted is our best two-planet Keplerian model (orange line), calculated from the best-fit orbital parameters of Table 4. *Lower panel:* Residuals of the best-fit two-planet model.

Orbital parameters and uncertainties for the KELT planets were determined with a Bayesian differential evolution Markov chain Monte Carlo analysis (e.g. Desidera et al. 2014). We adopted a two-planet Keplerian model with sixteen free parameters[4], assuming for KELT-6 b Gaussian priors on T_0 and P based on the new ephemeris. Fitted and derived parameters are listed in Table 4. The best-fit model is shown in Fig. 2, and the residuals show a dispersion of $\sim$17 m s^{-1}, which reduces to 9.5 m s^{-1} when considering only the more precise HIRES and HARPS-N measurements. This fact agrees nicely with the level of the activity-related jitter predicted by Santos et al. (2000).

KELT-6 c appears to be massive ($M_p$sin i=3.71±0.21 M_{Jup}) and moves on a moderately eccentric orbit (significant at the $\sim$5σ level) with period $P \sim$3.5 years. Residuals of the two-planet model do not reveal evidence of any trend of having a third companion (Fig. 2). Our results suggest that KELT-6 b has a likely circular orbit, with the eccentricity $e = 0.029^{+0.016}_{-0.013}$ compatible with zero within $\sim$2.45σ (Lucy & Sweeney 1971). A reanalysis of the data done by the KELT team corrected the eccentricity to the value e=0.058±0.034, which is in accordance with our measurement.

5.2. The Rossiter-McLaughlin effect for KELT-6 b

The RV time series covering the transit of KELT-6 b was analysed using the numerical model and the least-squares fitting algorithm described in Covino et al. (2013) and Esposito et al. (2014). Four parameters were set free[5], while all other relevant parameters were kept fixed to the values derived from the spectroscopic and photometric analyses. The best-fit values are reported in Tables 1 and 4, together with their uncertainties derived

---

[4] The central transit epoch T_0, the orbital period P, the RV semi-amplitude K, $\sqrt{e} \cos\omega$, and $\sqrt{e} \sin\omega$ of both planets KELT-6 b and KELT-6 c (e and ω being the eccentricity and the argument of periastron); a jitter term and a RV offset for each of the different datasets.
[5] γ: barycentric RV at mid-transit epoch; λ: projected angle between the planetary orbital axis and the stellar spin axis; $V \sin I_*$: projected stellar rotational velocity; μ: limb-darkening coefficient of a linear law.

Table 4. Orbital and physical parameters for KELT-6 b and KELT-6 c.

Parameter	KELT-6 b	KELT-6 c
Primary transit analysis		
T_c [BJD$_{\rm TDB}$ − 2,450,000]	7124.50954 ± 5.7 · 10^{-4}	
P [days]	7.845582 ± 7 · 10^{-6}	
$(R_{\rm p}/R_{\rm s})^a$	$0.077613^{+0.0010}_{-0.0009}$	
$b^{a,b}$	$0.20^{+0.14}_{-0.13}$	
$i^{a,c}$ [deg]	$88.81^{+0.79}_{-0.91}$	
RV analysis		
P^d [days]	7.8455821 ± 7 · 10^{-6}	1276^{+81}_{-67}
K^d [m s^{-1}]	41.8 ± 1.1	$65.7^{+2.6}_{-2.4}$
e^e	$0.029^{+0.016}_{-0.013}$	$0.21^{+0.039}_{-0.036}$
$(\sqrt{e}\sin\omega)^d$	$-0.083^{+0.120}_{-0.086}$	-0.454 ± 0.042
$(\sqrt{e}\cos\omega)^d$	$0.126^{+0.035}_{-0.046}$	-0.011 ± 0.071
ω^e [deg]	308^{+30}_{-272}	268.7 ± 8.8
$T_c{}^d$ [BJD$_{\rm TDB}$ − 2,450,000]	7124.50954 ± 5.8 · 10^{-4}	7432^{+39}_{-32}
$\gamma_{\rm TRES}{}^d$ [m s^{-1}]	46.3 ± 3.8	
$\gamma_{\rm HIRES}{}^d$ [m s^{-1}]	22.1 ± 8.5	
$\gamma_{\rm HARPS-N}{}^d$ [m s^{-1}]	1128.9 ± 3.0	
$(jitter_{\rm TRES})^d$ [m s^{-1}]	14.2 ± 4.5	
$(jitter_{\rm HIRES})^d$ [m s^{-1}]	$8.1^{+2.3}_{-1.8}$	
$(jitter_{\rm HARPS-N})^d$ [m s^{-1}]	2.2 ± 1.2	
$(M_{\rm p}\sin i)^{e,f}$ [M$_{\rm Jup}$]	0.442 ± 0.019	3.71 ± 0.21
$R_p{}^g$ [R$_{\rm Jup}$]	1.18 ± 0.11	
$a_{\rm p}{}^h$ [AU]	0.080±0.001	2.39 ± 0.11
$\gamma_{RM}{}^i$ [m s^{-1}]	1190.1 ± 1.4	
λ^i [deg]	−36±11	

Notes. $^{(a)}$ Co14 $^{(b)}$ Impact parameter. $^{(c)}$ Inclination of the orbital plane. $^{(d)}$ Fitted. $^{(e)}$ Derived. $^{(f)}$ For KELT-6 b this corresponds to the real mass of the planet, derived by assuming the best estimate of the inclination angle of the orbital plane provided by Co14. $^{(g)}$ Derived from the transit parameter $R_{\rm p}/R_{\rm s}$ in Co14 and our value of $R_{\rm s}$ through a Monte-Carlo analysis. $^{(h)}$ Derived from the third Kepler's law through a Monte-Carlo analysis, using our updated values for the stellar mass and planetary orbital periods. $^{(i)}$ Fitted (Rossiter-McLaughlin effect).
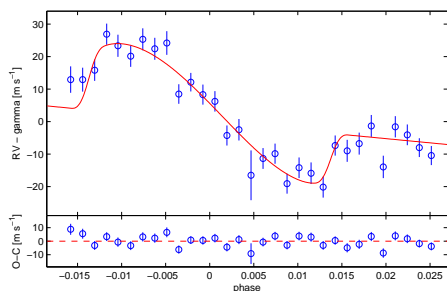

Fig. 4. HARPS-N RV time series spanning the transit of KELT-6 b occurred on 2015 April 11 (open blue circles) and our best-fit model of the Rossiter-McLaughlin effect (red solid line).

by means of a bootstrapping method. The best-fit RM model is shown in Fig. 4. Results show that KELT-6 b moves in a prograde orbit and is slightly misaligned with respect to the stellar spin axis with a projected spin-orbit angle $\lambda = -36° \pm 11°$. The lack of enough RV data in the pre-transit phase means that a value of λ closer to zero cannot be completely ruled out, but our solution comes with a lower χ^2 than for the case of λ fixed to 0 (1.39 *vs.* 1.89).

6. Discussion

KELT-6 joins a small number of host stars with a transiting planet and a measured RM effect for which there is evidence of outer companions. To our knowledge they are HAT-P-13, HAT-P-17, and WASP-8 (Knutson et al. 2014), the last two hosting a transiting planet with the orbital period close to that of KELT-6b (respectively, P=10.3 and 8.2 days) and with WASP-8 being mis-

aligned ($\lambda = -123.3^{+3.4}_{-4.4}$)[6]. Our results allow the description of the KELT-6 system architecture in some detail, and considerations can be made about its dynamical evolution and stability.

We tested the coplanar high-eccentricity migration hypothesis (CHEM, Petrovich 2015a) as a possible mechanism to explain the current orbital elements of KELT-6. CHEM explores the possibility that hot Jupiters are formed through secular gravitational interactions with an outer planet on an initial eccentric orbit, and then circularized by tides with the host star at periastron. The mechanism describes the planetary migration as occurring on nearly the same plane where the planets formed, assuming a low mutual inclination of the orbital planes ($\lesssim 20°$), and it predicts that hot Jupiters should have distant and more massive companions with moderately high eccentricities ($e \sim 0.2$-0.5). CHEM reproduces the observed architecture of KELT-6, provided that the inner planet, initially with $e \gtrsim 0.5$, started migration inside ~ 1 au, and there was an initial moderate mutual inclination of $\sim 10°$-$20°$ to account for the measured angle λ. This suggests that the current mutual inclination of the orbital planes could be lying in this range. We note that the system should be old enough for the orbit of KELT-6b to have been circularized. In fact, the circularization time with the current system parameters is about 0.45 Gyr, assuming a modified tidal quality factor $Q'_{\rm p} = 10^5$ for the planet (Lainey et al. 2009), where most of the tidal dissipation is expected to have occurred in the case of an initially eccentric orbit (see Jackson et al. 2008). We speculate that the initial conditions required by CHEM to explain this system could be the result of a preceding phase of planet-planet scattering. A system with more than two planets in nearly circular and coplanar orbits at $\gtrsim 1$ au might have become unstable, losing planets by ejections and leading to eccentricity excitation and moderate change (by a factor up to ~ 2) in the semi-major axis of the inner planet (Jurić & Tremaine 2008; Chatterjee et al. 2008).

We investigated the dynamical stability of the KELT-6 system by using the empirical relation (17) in Petrovich (2015b), who studied the final results of the evolution on long timescales of two-planet systems with arbitrary eccentricities and mutual inclinations against either ejections or collisions with the host star. We found that the relation is satisfied well, implying a stability preserved on a timescale of a few Myr (i.e. the range of validity of Petrovich's formula), as expected for a system that is already ~ 5 Gyr old.

References

Baranne, A., Queloz, D., Mayor, M., et al. 1996, A&AS, 119, 373
Biazzo, K., D'Orazi, V., Desidera, S., et al. 2012, MNRAS, 427, 2905
Brewer, J. M., Fischer, D. A., Basu, S., Valenti, J. A., & Piskunov, N. 2015, ApJ, 805, 126
Buchhave, L. A., Bakos, G. Á., Hartman, J. D., et al. 2010, ApJ, 720, 1118
Castelli, F. & Kurucz, R. L. 2004, arXiv:astro-ph/0405087
Chatterjee, S., Ford, E. B., Matsumura, S., & Rasio, F. A. 2008, ApJ, 686, 580
Claret, A. & Bloemen, S. 2011, A&A, 529, A75

---

[6] see http://www.astro.keele.ac.uk/jkt/tepcat/rossiter.html

Collins, K. A., Eastman, J. D., Beatty, T. G., et al. 2014, AJ, 147, 39
Cosentino, R., Lovis, C., Pepe, F., et al. 2012, in Society of Photo-Optical Instrumentation Engineers (SPIE) Conference Series, Vol. 8446, Society of Photo-Optical Instrumentation Engineers (SPIE) Conference Series
Covino, E., Esposito, M., Barbieri, M., et al. 2013, A&A, 554, A28
Damasso, M., Biazzo, K., Bonomo, A. S., et al. 2015, A&A, 575, A111
Demarque, P., Woo, J.-H., Kim, Y.-C., & Yi, S. K. 2004, ApJS, 155, 667
Desidera, S., Bonomo, A. S., Claudi, R. U., et al. 2014, A&A, 567, L6
Dumusque, X., Bonomo, A. S., Haywood, R. D., et al. 2014, ApJ, 789, 154
Esposito, M., Covino, E., Mancini, L., et al. 2014, A&A, 564, L13
Fűresz, G. 2008, PhD thesis, Univ. of Szeged, Hungary
Gandolfi, D., Parviainen, H., Deeg, H. J., et al. 2015, A&A, 576, A11
Jackson, B., Greenberg, R., & Barnes, R. 2008, ApJ, 678, 1396
Jurić, M. & Tremaine, S. 2008, ApJ, 686, 603
Knutson, H. A., Fulton, B. J., Montet, B. T., et al. 2014, ApJ, 785, 126
Kurucz, R. L. 1992, in The Stellar Populations of Galaxies: Proceedings of the 149th Symposium of the International Astronomical Union, 225
Lainey, V., Arlot, J.-E., Karatekin, Ö., & van Hoolst, T. 2009, Nature, 459, 957
Lucy, L. B. & Sweeney, M. A. 1971, AJ, 76, 544
Nascimbeni, V., Cunial, A., Murabito, S., et al. 2013, A&A, 549, A30
Nascimbeni, V., Piotto, G., Bedin, L. R., & Damasso, M. 2011, A&A, 527, A85
Ohta, Y., Taruya, A., & Suto, Y. 2005, The Astrophysical Journal, 622, 1118
Pepe, F., Mayor, M., Galland, F., et al. 2002, A&A, 388, 632
Petrovich, C. 2015a, ApJ, 805, 75
Petrovich, C. 2015b, arXiv:1506.05464
Santerne, A., Díaz, R. F., Bouchy, F., et al. 2011, A&A, 528, A63
Santos, N. C., Mayor, M., Naef, D., et al. 2000, A&A, 361, 265
Sneden, C. 1973, Astrophysical Journal, 184, 839
Sousa, S. G., Santos, N. C., Adibekyan, V. Z., Delgado Mena, E., & Israelian, G. 2015, A&A, 577, A67
Sousa, S. G., Santos, N. C., Israelian, G., Mayor, M., & Udry, S. 2011, 533, A141
Southworth, J. 2008, MNRAS, 386, 1644
Southworth, J. 2011, MNRAS, 417, 2166
Sozzetti, A., Torres, G., Charbonneau, D., et al. 2007, ApJ, 664, 1190
Torres, G., Fischer, D. A., Sozzetti, A., et al. 2012, ApJ, 757, 161
Valenti, J. A. & Piskunov, N. 1996, A&AS, 118, 595

[1] INAF – Osservatorio Astrofisico di Torino, Via Osservatorio 20, I-10025, Pino Torinese, Italy.
E-mail: damasso@oato.inaf.it

[2] Instituto de Astrofísica de Canarias, C/Via Láctea S/N, E-38200 La Laguna, Tenerife, Spain

[3] Departamento de Astrofísica, Universidad de La Laguna, E-38205 La Laguna, Tenerife, Spain

[4] INAF – Osservatorio Astronomico di Padova, Vicolo dell'Osservatorio 5, I-35122, Padova, Italy

[5] Dip. di Fisica e Astronomia Galileo Galilei – Università di Padova, Vicolo dell'Osservatorio 2, I-35122, Padova, Italy

[6] Harvard-Smithsonian Center for Astrophysics, Cambridge, MA 02138 USA

[7] INAF – Osservatorio Astrofisico di Catania, Via S.Sofia 78, I-95123, Catania, Italy

[8] INAF – Osservatorio Astronomico di Capodimonte, Salita Moiariello 16, I-80131, Napoli, Italy

[9] Dipartimento di Fisica, Università di Torino, via P. Giuria 1, 10125 Torino, Italy

[10] Landessternwarte Königstuhl, Zentrum für Astronomie der Universität Heidelberg, Königstuhl 12, D-69117 Heidelberg, Germany

[11] INAF – Osservatorio Astronomico di Brera, Via E. Bianchi 46, I-23807 Merate (LC), Italy

[12] Department of Astrophysical Sciences, Princeton University, Ivy Lane, Princeton, NJ 08544, USA

[13] Department of Physics and Astronomy, Vanderbilt University, Nashville, TN 37235, USA

[14] Department of Physics and Astronomy, University of Louisville, Louisville, KY 40292, USA

[15] Fundación Galileo Galilei - INAF, Rambla José Ana Fernandez Pérez 7, E-38712 Breña Baja, TF - Spain

[16] INAF – Osservatorio Astronomico di Palermo, Piazza del Parlamento, 1, I-90134, Palermo, Italy

[17] INAF - IASF Milano, via Bassini 15, I-20133 Milano, Italy

[18] INAF – Osservatorio Astronomico di Trieste, via Tiepolo 11, I-34143 Trieste, Italy

[19] Universidad de Atacama, Departamento de Fisica, Copayapu 485, Copiapo, Chile

[20] Max Planck Institute for Astronomy, Königstuhl 17, 69117 – Heidelberg, Germany

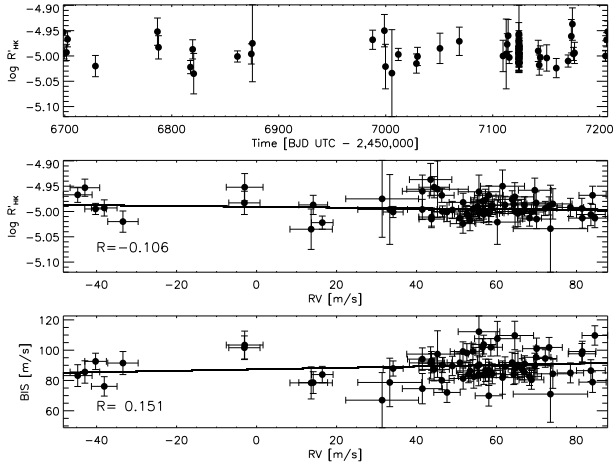[21] Astrophysics Group, Keele University, Staffordshire, ST5 5BG, UK

Fig. 3. (*Upper panel*). Time series of the log(R′$_{HK}$) chromospheric index as measured from HARPS-N spectra. (*Middle and lower panels*). Correlation analysis between the RV residuals, obtained by removing the Keplerian signal due to KELT-6 b from the original HARPS-N dataset, and two indicators of stellar activity derived from the HARPS-N spectra: the log(R′$_{HK}$) chromospheric index and the CCF bisector span. Overplotted are the values of Spearman's rank correlation coefficients, which show the absence of significant correlations and support the hypothesis that the origin of the observed RV long-term variations is Keplerian.

Table 2. Sample list of all the radial velocities (RV) measured for KELT-6 with the HARPS-N spectrograph in the framework of the GAPS programme. Also indicated are the bisector velocity span (BIS) and the activity index log(R′$_{HK}$). The BIS are those derived by the data reduction pipeline of HARPS-N with uncertainties assumed to be twice those on the radial velocities.

Time (BJD$_{UTC}$ - 2,450,000)	RV (m s^{-1})	RV err. (m s^{-1})	BIS (m s^{-1})	log(R'_{HK})	log(R'_{HK}) err.
6698.624617	1127.6	3.7	85.6	-4.953	0.017
6699.598118	1124.1	2.7	92.6	-4.995	0.011
6701.572178	1069.7	3.2	76.1	-4.993	0.016
6702.578027	1044.5	3.6	83.2	-4.967	0.015
6728.651408	1105.1	3.8	91.5	-5.020	0.021
6786.609623	1143.6	4.6	103.4	-4.952	0.027
6787.608024	1112.3	3.9	101.6	-4.983	0.023
6817.482897	1176.6	2.7	83.9	-5.022	0.013
6819.529437	1115.1	3.6	78.6	-4.987	0.019
6820.503665	1101.6	5.3	78.4	-5.035	0.040
6861.396206	1150.9	2.5	87.9	-5.001	0.011
6874.367191	1144.3	3.7	94.1	-4.996	0.020
6875.369909	1119.5	9.1	67.0	-4.975	0.076
6987.775868	1204.0	3.6	86.8	-4.968	0.019
6998.737459	1198.9	5.5	81.9	-4.950	0.032
6999.772079	1166.2	5.7	107.6	-5.021	0.044
7005.756862	1234.1	9.3	71.0	-5.034	0.086
7011.773901	1226.4	2.7	90.9	-4.997	0.012
7028.700777	1240.1	3.5	101.0	-5.015	0.019
7029.691968	1216.8	3.5	87.4	-5.001	0.018
7050.675470	1224.3	4.8	84.4	-4.985	0.030
7068.780530	1218.8	4.7	109.7	-4.971	0.028
7109.622389	1170.3	5.0	87.8	-5.000	0.031
7112.604654	1155.1	8.0	78.7	-4.996	0.069
7113.520997	1209.9	3.7	86.7	-4.977	0.021
7114.443438	1212.0	5.0	74.6	-4.960	0.032
7115.451479	1219.3	2.6	90.4	-5.003	0.012
7124.384992	1203.2	4.1	89.8	-4.958	0.024
7124.395594	1203.2	3.7	95.3	-4.983	0.022
7124.406149	1206.1	3.3	101.8	-4.989	0.018
7124.416785	1217.2	3.2	109.7	-5.013	0.019
7124.427595	1213.6	3.4	97.6	-4.994	0.020
7124.438266	1210.4	3.3	85.0	-4.992	0.018
7124.448937	1215.6	3.4	78.9	-4.968	0.018
7124.459481	1212.7	3.4	99.1	-5.013	0.020
7124.470175	1214.5	3.6	86.5	-5.006	0.022
7124.481309	1198.8	3.0	82.7	-5.013	0.016
7124.491679	1202.4	2.9	94.5	-4.994	0.014
7124.502581	1198.6	3.1	80.4	-5.001	0.016
7124.513125	1196.5	3.2	85.3	-4.987	0.016
7124.524155	1186.0	3.1	83.6	-5.006	0.016
7124.534618	1187.8	3.3	84.4	-4.988	0.018
7124.543668	1173.8	7.7	97.4	-4.956	0.056
7124.556156	1179.0	3.2	91.7	-5.013	0.018
7124.566665	1180.4	3.1	98.1	-5.005	0.017
7124.577441	1171.2	3.1	92.9	-5.015	0.017
7124.587949	1176.1	3.2	89.6	-4.997	0.017
7124.599130	1174.4	3.3	72.1	-5.001	0.019
7124.609685	1170.2	3.2	91.4	-5.011	0.018
7124.620229	1182.9	3.1	103.7	-4.998	0.017
7124.631085	1181.3	3.4	83.3	-4.996	0.018
7124.641640	1183.5	3.4	69.9	-5.002	0.018
7124.652496	1189.0	3.4	91.8	-4.976	0.017
7124.663202	1176.4	3.5	81.3	-4.982	0.018
7124.673908	1188.7	3.3	83.9	-4.985	0.016
7124.684347	1186.2	3.2	89.2	-4.987	0.017
7124.695354	1182.3	2.9	101.9	-4.995	0.015
7124.705932	1179.9	2.9	101.8	-4.980	0.015
7142.537170	1144.0	3.6	89.5	-4.990	0.021
7143.470202	1158.9	3.4	86.3	-5.018	0.020
7144.467594	1196.6	3.8	84.4	-5.003	0.023
7150.499394	1155.1	4.6	90.2	-5.004	0.026
7159.414630	1164.7	3.2	99.1	-5.024	0.019
7170.469914	1214.6	2.7	83.9	-5.010	0.012
7173.479806	1143.8	5.2	112.2	-4.961	0.033
7174.499116	1140.4	5.3	91.6	-4.937	0.032
7175.462458	1179.1	2.7	99.2	-4.996	0.013
7176.476235	1212.3	3.8	82.5	-4.994	0.021
7205.414495	1136.2	2.5	90.2	-5.000	0.011
7206.421521	1157.3	3.1	80.1	-4.968	0.014
7207.432852	1189.7	3.8	87.3	-4.952	0.021

Table 3. List of the new relative radial velocities of KELT-6 measured with the TRES spectrograph and used for the first time in this work.

Time (BJD$_{UTC}$ - 2,450,000)	RV (m s^{-1})	RV error (m s^{-1})
6640.021901	-30.50	36.12
6643.998845	35.66	23.47
6698.953413	86.48	24.29
6702.883586	-15.28	28.33
6729.914621	64.77	24.93
6733.902128	4.10	19.52
6801.709729	59.28	22.98
6803.711379	-15.48	12.28
6804.800386	-14.19	22.87
6812.690753	54.72	29.16
6816.685639	73.70	18.88
6824.685293	94.65	14.15
6993.029954	107.42	22.14
7055.946535	94.92	18.22
7090.798944	172.10	19.99
7094.908058	101.59	19.32
7110.916771	73.25	20.13
7121.849369	133.02	17.07
7141.862950	35.84	17.49
7145.767451	156.82	17.82
7149.696112	42.03	18.32
7169.684005	133.14	18.14